



Contents lists available at ScienceDirect

Arabian Journal of Chemistry

journal homepage: www.ksu.edu.sa

A convergent fabrication of graphene oxide/silk fibroin/hydroxyapatite nanocomposites delivery improved early osteoblast cell adhesion and bone regeneration

Xi Li^a, Abdurahman Hajinur Hirad^b, Abdullah A. Alarfaj^b, Hua Li^a, Rameshkumar Santhanam^{c,*}

^a Department of Orthopaedics, The First Affiliated Hospital of Kunming Medical University, Kunming 650000, China

^b Department of Botany and Microbiology, College of Science, King Saud University, P. O. Box.2455, Riyadh 11451, Saudi Arabia

^c Faculty of Science and Marine Environment, Universiti Malaysia Terengganu, Kuala Nerus 21030, Terengganu, Malaysia

ARTICLE INFO

Keywords:

Drug delivery
Graphene
Silk fibroin
Hydroxyapatite
Calvarial defect
Bone regeneration

ABSTRACT

For controlled bone regeneration, two-dimensional materials are essential because they provide an isolated area for bone regeneration and protect the surrounding tissues. Excellent mechanical and hydrophilic qualities have made graphene oxide (GO) a common choice for bone regeneration. A biomimetic mineralization process combined with one-step vacuum filtering created mechanically strong and biocompatible two-dimensional (2D) membranes. Silk fibroin (SF) and hydroxyapatite (HA) increased the membranes' mechanical strength and hydrophilicity on the surface. Osteoblast adhesion, differentiation, and mineralization improved with little HA administered. A calvarial defect model was used to test the impact of the produced composite membranes on bone formation in vivo after they were implanted. Histological examination demonstrates that bone regeneration may be accelerated by GO/SF/HA composite membranes without needing endogenous cytokines. GO/SF/HA nanocomposite membranes with distinctive porous architectures, exceptional mechanical characteristics, and excellent bone regeneration capability are viable nanocomposites for bone regeneration.

1. Introduction

Bone regeneration is among the most pressing issues we face daily. In the immediate aftermath of tooth extraction, the alveolar bone undergoes typical biological processes that restrict future implant placement options in some circumstances (Zhai et al., 2020). In recent years, various methods for preserving bone have been tested. Creating the essential bone structure for a patient's occlusal rehabilitation is more difficult in trauma, tumor removal surgery, or congenital malformations because of the increased technical and biological demands (Abbasi et al., 2020). In bone volume, numerous ways have been offered to promote implant osteointegration or improve a patient's bone structure where it would be implanted. There is still high regard for autogenous bone transplant due to its superiority in osteogenesis and osteoconduction. Some drawbacks include the necessity for further operation, limited supply, and morbidity in the donor location (Zhu et al., 2020). Allogeneic grafts, xenogeneic grafts, and alloplastic biomaterials with

osteoconductive potential have been presented as alternative biomaterials. These materials are appropriate but aren't ideal (Bai et al., 2018; O'Neill et al., 2018; Glenske et al., 2018). Additional drawbacks include resttumorriccted quantities, and quality of bone grafts made possible using these materials. Silk fibroin nanofibers, generally in the form of a composite with hydroxyapatite, have been synthesized using various methods, including electrospinning and biomimetic mineralization (Sbricoli et al., 2020). Using blending spinning and alternating soaking, Kim et al. fabricated composite nanofibers (Zhu et al., 2020). Moreover, the composite has more excellent mechanical qualities than comparable scaffolds from pure silk fibroin (Lee et al., 2019). Cell adhesion, proliferation, differentiation, and mineralization are all boosted by incorporating hydroxyapatite into the composites (Bai et al., 2020; Takeuchi et al., 2019; Armiento et al., 2020). Although hydroxyapatite enhances mechanical characteristics and biocompatibility, bone-like scaffolds have yet to be developed (Shuai et al., 2020). The biocompatibility and cytotoxicity of the many nanotechnologies used in

Peer review under responsibility of King Saud University.

* Corresponding author at: Faculty of Science and Marine Environment, Universiti Malaysia Terengganu, Kuala Nerus 21030, Terengganu, Malaysia.

E-mail address: ramesh@umt.edu.my (R. Santhanam).

<https://doi.org/10.1016/j.arabjc.2023.105468>

Received 21 July 2023; Accepted 18 November 2023

Available online 19 November 2023

1878-5352/© 2023 The Authors. Published by Elsevier B.V. on behalf of King Saud University. This is an open access article under the CC BY-NC-ND license (<http://creativecommons.org/licenses/by-nc-nd/4.0/>).

bone regeneration remain a concern, notwithstanding the advances gained thus far (Gisbert-Garzarán et al., 2023). Reactive oxygen species (ROS) produced at high cell levels are the primary mechanism behind nanotoxicity (Lee et al., 2023). ROS can damage cells and lead to subsequent dysfunctions of the cellular microenvironment via downstream effects like peroxidizing lipids, damaging DNA, and changing gene transcription. In contrast to conventional chemical toxicants, nanomaterials cannot have their toxicity ultimately determined by analyzing their purity and chemical makeup (Bagchi et al., 2014). The intricacy of comprehending nanotoxicity is further increased because it is yet unclear why nanomaterials differ in toxicity from their bulk counterparts (Huang et al., 2020).

Graphene oxide (GO) has recently gained significant attention in biological applications due to unique physicochemical features, including a large surface area, excellent dispersion, and water-loving capabilities. A substantial interfacial strength is predicted to be generated by the oxygen-containing functional groups found on the basal plane and edges of GO (Amiryaghoubi et al., 2021; Wright et al., 2019; Choe et al., 2019). This increased interfacial contact between GO and its polymer matrix will aid stress transmission from the polymer matrix to the GO molecule. GO's large surface area and abundance of functional groups make it an excellent chemical absorbent (Feng et al., 2020). Protein-GO interactions help osteogenic cell differentiation of progenitor cells through hydrophobic and electrostatic interactions. Nanomaterials based on GO and CHT have been fabricated for bone regeneration in various forms and applications (Jiao et al., 2021). They used the covalent bond of graphene's carboxylic group ($-\text{COOH}$) with the amino group ($-\text{NH}_2$) of biomaterials chitosan. Sumathra and co-workers have developed the chitosan/graphene system, which they found to improve the bio-responses of the osteoblasts, such as cell growth, proliferation, and attachment (Sumathra et al., 2018). In another study, Wu et al. initiated a biomimetic GO/SF scaffold that incorporates a BMP-2-incorporated bovine serum albumin (BSA) nanocomposites and an Ag nanomaterial (Ag-NMs)-absorbed biomimetic bone morphogenetic protein (BMP) (Wu et al., 2019). It was shown that the biomimetic scaffolds were biocompatible and induced bone tissue regeneration by increasing bone stromal cell proliferation and differentiation (Zhang et al., 2018; Wongpinyochit et al., 2019; Cheng et al., 2015). Kolanthai and his colleagues have developed a chitosan/alginate/collagen-based nanocomposite platform containing GO, which they claim can enhance osteoblast cell proliferation and osteogenic differentiation for bone tissue engineering (Zheng et al., 2021). Regarding bone tissue engineering, we don't know how functionalized GO and silk fibroin work together since we don't yet know how functionalized GO and silk fibroin interact.

Polymers of synthetic and natural origin, ceramics, metals, or even a mixture of these materials have been used to achieve the desired properties (Zheng et al., 2021). The employment of ceramic materials with natural polymers, including collagen, fibroin, chitosan, starch, and alginates, notably in bone tissue applications, has been particularly notable (Zhang et al., 2018). Serine, glycine, and alanine make up to 90 % of silk fibroin, a natural protein that forms crystalline-pleated sheets in silk fiber (Wessing et al., 2018; Metwally et al., 2020; Wang et al., 2019). Silk is a viable alternative for bone tissue engineering because of its natural strength, biocompatibility, biodegradability, water and oxygen permeability. On the other hand, SF is too rigid and brittle to be employed as a biomaterial scaffold. Silk fibroin cannot be used to fabricate porous scaffolds, making it challenging to include bioactive elements. Blending silk fibroin with other natural or synthetic polymers is possible beyond the described restriction (Sun et al., 2021). To develop graphene oxide (GO), we first need graphene. Since its large surface area, good biocompatibility, biostability, electrical, thermal, and mechanical properties, and the ease with which it can be chemically modified, graphene—a two-dimensional (2D) honeycomb lattice of carbon atoms with a high aspect-ratio layer geometry—has gotten a lot of attention recently (Wang et al., 2020; Wang et al., 2020; Wang et al.,

2020). Graphene sheets have been employed in biotechnology, from bacterial inhabitation to cancer-targeting to cellular imaging, biosensor development to developing antiviral materials, drug delivery, and tissue engineering (Wu et al., 2022; Wang et al., 2021; Narimani et al., 2019; Sun et al., 2019). Graphene-based polymer nanocomposites have recently enhanced polymers' thermal, electrical, and mechanical characteristics. In tissue engineering, GO might fabricate biomimetic scaffolds (Moe et al., 2022). An oxygen-containing functional group in the basal plane and edges, such as epoxy, hydroxyl, or carboxyl, gives GO excellent hydrophilicity and cell adsorption properties. Because of the wrinkled shape of the carbon plane, GO has been shown to increase stem cell adhesion and stimulate stem cell development from osteoblast lineage (Ou et al., 2019). Because of GO's enormous surface area and abundance of functional groups, it is an excellent absorbent for many chemicals (Eivazzadeh-Keihan et al., 2020). According to recent studies, the biocompatibility and mechanical qualities of the finished goods can be improved by using GO (Zhao et al., 2021).

These GO/SF/HA nanocomposite membranes were fabricated by the biomimetic mineralization process and one-step vacuum filtration to provide the mechanical strength and flexibility of a 2D membrane that promotes cell adhesion in bone regeneration. With SF and HA, the fabricated composite membranes likewise had a multilayered design. The initial step was to define the membranes' shape and individual constituents. Finally, the hydrophilic and mechanical characteristics of this nanocomposite membrane were studied. SF and HA improved both their hydrophilicity and surface mechanical characteristics. As a next step, MG-63 osteoblast precursor cells were incubated with composite membranes to evaluate their adhesion, proliferation, differentiation, and mineralization. The calvaria defect model tested the nanocomposite membrane's potential to promote in vivo bone regeneration.

2. Methods and materials

2.1. Materials

All materials and reagents were used as received with no further purification. *B. Mori* silkworm cocoons were purchased from the Shandong Academy of Sericulture, China. CaCl_2 (98 %), Na_2HPO_4 (99.9 %), and other chemical reagents used here were of analytical grade and purchased from Sinopharm Chemical Reagents Co. Ltd., China. Deionized water was used throughout the experiment. Graphite (99.9 %) and Hydroxyapatite (HA, 99.5 %) were purchased from XFANO Materials Tech Co. Ltd (Nanjing, China). RPMI-1640 medium (99.9 %) and fetal bovine serum (FBS, 99.9 %) were purchased from Gibco Invitrogen. 3-(4,5-Dimethylthiazol-2-yl)-2,5-diphenyltetrazolium bromide (MTT, 99.9 %) and alkaline phosphatase (ALP) kit was acquired from Boster Bio-Tech Co. Ltd (Wuhan, China).

Mouse osteoblast cells (MG-63) were purchased from the Chinese Academy of Sciences (Shanghai, China). All cells were cultured in DMEM medium supplemented with 10 % fetal bovine serum at 37 °C incubated with 5 % CO_2 . The animal experiments complied with national guidelines and the care and use of laboratory animals. Chengdu Dashuo Biotechnology Co., Ltd provided the animals.

2.2. Characterization

The size and morphology of all nanocomposites were characterized by transmission electron microscopy (HT7700, TEM) with an acceleration voltage of 100 kV. The morphologies of nanocomposites were investigated using a scanning electron microscope (SEM) (Zeiss Gemini Sigma 300 VP, Germany). The catalyst's element mapping was carried out using an energy-dispersive X-ray spectrometer (EDS) with a scanning electron microscope. Nanocomposites' Fourier transform infrared (FT-IR) spectra were recorded using a Nicolet 6700 FT-IR Spectrometer (Thermo Fisher, USA). Raman spectra were measured at room temperature with a Jobin-Yvon T64000 triple-stage spectrograph with a

spectral resolution of 2 cm^{-1} . Tensile testing was done using a Hounsfield universal test machine at a cross-head speed of 0.5 mm s^{-1} . The contact angles of the electrospun mats were measured with a drop shape analysis system (Krüss DSA100) in the sessile mode at room temperature. Cell viability at 570 nm by a microplate reader Synergy HTX Multi-Mode Microplate Reader, BioTek). Fluorescence microscopy (Olympus, CKX53) was used to take cell images after the samples had been washed with PBS.

2.3. Preparation of silk fibroin and GO nanosheets

The sericin in silkworm cocoons was removed by cooking them in a Na_2CO_3 (0.02 M) solution for 30 min after being cut open with scissors. Removed by deionized water, dried for a night, and dissolved in a LiBr (9.3 M) solution for 2 h at 60°C to remove contaminants. A dialysis membrane (rated at 3500 W) was used to dialyze the dissolving yellow viscous liquid for three days, changing the deionized water every 8 h. For 20 min, the solution was spun at 4000 rpm in a centrifuge tube after dialysis to remove any remaining waste product. Soap made up the supernatant that had been collected. With deionized water, 10 % of the mass volume fraction was diluted to 5 %. Afterward, it was placed in a freezer at 4°C for future usage.

We used the Hummers and Offeman technique to develop GO using powdered flake graphite as a starting point (Feicht et al., 2019). A beaker of sulfuric acid was placed in an ice bath and agitated. The graphite flake powder and sodium nitrate solutions were progressively poured into the flask to fabricate the GO suspension. After the ice bath was withdrawn, the suspension climbed to 35°C after 5 min of stirring. After that, the mixture was stirred for another 30 min. For 15 min, the mixture was mixed with deionized water. H_2O_2 (30 %) was progressively added to remove the foam from the suspension. GO nanoplatelets were obtained by washing the dispersion with deionized water and freeze-drying.

2.4. Fabrication of GO/SF/HA membranes

Silk fibroin solution (2 mg/mL) was made by dissolving silk fibroin (SF) in 1 mol/L acetic acid and stirring it for 6 h. Ultrasonic dissolving produced a GO suspension with a 1 mg/mL concentration. The SF solution and GO suspension were combined in a 3:1 vol ratio and swirled for 48 h. Vacuum filtering was used to fabricate GO/SF composite membranes from a liquid mixture. To prepare the simulated body fluid (SBF) using a solution of distilled water, KCl and NaCl were mixed with a specific concentration of these salts at 37°C . Later, the solution was treated further by adding NaHCO_3 and HCl. Finally, tris(hydroxymethyl) aminomethane was used to adjust the pH of the solution to 7.4. SBF was used to amplify a $1.5 \times$ SBF solution fabricated similarly. Then, the GO/SF membranes were submerged in $1.5 \times$ SBF and SBF for days 1, 3, and 7 to produce the nanocomposite membranes.

2.5. Cell proliferation on MG-63

The Mouse osteoblasts (MG-63) were cultured in RPMI-1640 medium with 10 % fetal bovine serum (FBS) and 1 % penicillium-streptomycin antibiotics. The cells were incubated for 24 h in humidified conditions inside the incubator at 37°C and 5 % CO_2 . MG-63 was seeded with various samples at 3×10^4 cells/well concentration in two 24-well plates containing 11 mm glass coverslips inside each well. The viability of the cells was then determined by measuring the absorbance at 570 nm with a microplate reader. Fibronectin staining with a fluorescence microscope assessed cell spreading and attachment at 1 and 3 days (Subarkhan and Ramesh, 2016; Mohamed Kasim et al., 2018; Kalaiarasi et al., 2022; Giriraj et al., 2022; Sathiyaa Kamatchi et al., 2020).

2.6. Investigations of ALP activity and the mineralization

The osteogenic differentiation of MG-63 cells depended on alkaline phosphatase (ALP) (Vimalraj, 2020; Wang et al., 2020). We initiated using composite membranes by growing 1×10^4 cells in 48-well plates for 7, 10, and 14 days. For ALP activity measurement, supernatants followed the manufacturer's instructions after cells had been lysed with Triton X-100. As MG-63 cells progress through osteogenic differentiation, mineralization becomes evident and may be seen using alizarin red staining of the cell lysates. For 21 days, cells were grown on 24-well plates in the same way as described before. Once the cells had been fixed, an alizarin red solution was used to color the membranes of the cells. Nodules stained with mineralization staining were quantified using cetylpyridinium chloride and 570 nm absorbance.

2.7. Animal experiments

The 8-week SD rats (male) were purchased from Caven's animal center (Changzhou, China) and kept in the center's SPF house with free access to diet. All animal experiments were conducted under the supervision of the Animal Ethics Committee of the Department of Orthopaedics, The First Affiliated Hospital of Kunming Medical University, Kunming, 650000, China, and strictly followed the NIH guidelines for the care and use of experiment animals. It was tested in a rat (male) calvaria defect model to determine composite membranes' ability to promote osteogenesis. Animals were prepared for surgery by anesthetizing them with an intramuscular injection of a mixture of ketamine (100 mg/ml), xylazine (20 mg/ml), acepromazine (10 mg/ml), and saline in the ratio of 5:2.5:1:1.5; the animals were maintained under anesthesia during the entire surgical procedure. Through intraperitoneal administration, they were kept under anesthesia throughout the surgery. Membranes with a 5 mm diameter are disinfected before use. To remove any hair and bacteria from the epidermis on the cranium, it was necessary to use a trephine to make calvaria flaws with sizes of 5 mm. The membranes were then applied to the defect areas. Randomly, the four groups of calvaria defect rats were divided into the nonmembrane group (control), the GO/SF group, the GO/SF/HA group, and a sham-surgery group (Sham). Each experiment included a total of six rat subjects. After the procedure, surgical sutures were used to seal the subcutaneous tissue and the epidermis.

A general operating protocol was conducted, with the specimens decalcified, dehydrated, and paraformaldehyde. The inserted samples were then sliced into 5 μm -thick slices in the opposite direction of the bone. H&E staining was performed per standard procedure on the slices.

2.8. Hemolysis assay and the subcutaneous implantation of the membranes

The composite membranes were subjected to hemolysis to determine their blood safety. In a nutshell, several membranes were sliced into 1.5 cm^2 squares for utilization. A 2 % saline solution of fresh mice blood was prepared. A blood suspension of 2.5 mL at 37°C was added to the membranes. The negative control was PBS, while the positive control was water. It took four hours to centrifuge and collect the supernatant, which was then detected using a microplate reader. A prior study's technique was used to determine hemolysis (Fischer et al., 2003).

A subcutaneous implant was employed to screen the membranes' safety using an in vivo model. The mentioned method anesthetized these mice, and the membrane was inserted into the subcutaneous tissue. The heart, liver, kidney, spleen, lung, and tissues. After the animals' implantation site was 4 weeks post-operatively, the implantation site, heart, liver, kidney, spleen, and lung were dissected and fixed in neutral 10 % formalin, then examined with H&E staining.

3. Results and discussion

3.1. GO nanosheets characterization

GO's scanning electron microscopy (SEM) image reveals a rough surface and a wrinkled structure, like a leaf (Fig. 1A). The TEM shows that the surface of GO is folded (Fig. 1B). According to AFM imaging, GO had a thickness of around 1 nm (Fig. 1C, D). Graphite and GO nanosheet X-ray diffraction patterns are shown in this work (Fig. 1E). At 26.6° , the graphite's crystalline peak was recorded, with a d-spacing of 0.33 nm. Because graphite was transformed into graphene nanosheets in the presence of oxygen, the crystallographic peak of the GO was detected at 14.0° with 0.68 nm d-spacing. The G band (Raman G band) was the most prominent in graphite's Raman spectroscopy. Carbon-based materials with sp² hybridizations can be seen in this band. In addition to the D and G bands, GO had other sub bands (Fig. 1F). The D/G band intensities (ID/IG) ratio was used to assess the degree of oxidation in nanocarbon materials. The Raman spectrogram arrived at an ID/IG value of 0.89. The results of this study show that GO nanosheets have been effectively fabricated.

Several synthetic membranes were examined using FTIR spectra to determine their composition (Azerbaijan et al., 2021). These unique absorption peaks at 3402, 2987, 1601, and 1392 cm^{-1} demonstrate the absorbance of GO and SF alone, as illustrated in Fig. 2A. A compelling synthesis of membranes made from GO and SF is shown. The twisting, stretching, and vibration patterns of HA's PO_4^{3-} bands were seen in the FTIR spectrum of powdered HA on GO/SF membrane substrates. SBF and 1.5SBF composite membranes had FTIR patterns consistent with those of the individual membrane components. It is possible to explain the peaks at 3401 and 1599 cm^{-1} by the growth of GO's carboxyl and epoxy groups hydroxyl and imido group stretching vibrations may be found at 3510 cm^{-1} , 2901 cm^{-1} is extending vibrations of the methyl group, and 1380 cm^{-1} is stretching vibrations of the methyl group, respectively (Aleml et al., 2020). Experiments were conducted using XRD to determine the membranes' crystallinity (Fig. 2B). XRD patterns for HA-standard membranes were used to compare the peak heights of these two membranes. Fig. 2C, D shows the EDX mapping spectrum of an SBF@GO/SF/HA and 1.5SBF@GO/SF/HA. As can be seen, the EDX image has all the standard components in the final structure. The presence of O, P, Ca, and Mg in the EDX spectrum indicates that SBF@GO/

SF/HA is present. Graphene oxide and silk fibroin may also contribute to the carbon and oxygen content. Nitrogen in the EDX spectrum indicates that silk fibroin is present in the structure. The distribution of the elements was also assessed using elemental mapping images, and it was discovered that the distribution of the elements was acceptable.

3.2. Characterization of GO-based composite membranes

The one-step vacuum filtering procedure was used to manufacture GO and GO/SF membranes, then cut into various widths and bent in any direction, resulting in exceptional flexibility (Fig. 3A). The surfaces of GO/SF membranes were flat and wrinkled, showing multilayered structures (Fig. 3A). Additional measurements show that the membrane thicknesses are around 15 nm. SBF and 1.5 SBF were used to deposit and produce HA mineralization on the GO/SF membranes, and the membranes were then exposed to the solutions for one day. SBF and 1.5x SBF membranes were mineralized for 3 and 7 days, respectively, resulting in spherical raw material with 200 and 350 nm diameters on the surface of the membrane (Fig. 3B). Interestingly, compared with the 1.5SBF@GO/SF/HA membranes, the surfaces of the SBF@GO/SF/HA membranes had more wrinkled structures and were rougher. The roughness of the SBF@GO/SF/HA membranes was increased compared with that of the 1.5SBF@GO/SF/HA membranes, which supported the probability of improving cell adhesion (Fig. 3C). On top of that, the produced nanoparticles were exposed to various deposition times in various solutions, including SBF and $\times 1.5$ SBF, for respective days. Nanoparticles formed on GO/SF membranes after mineralization in SBF or 1.5 SBF were found to have a similar average size and number of particles, as shown by the findings (Fig. 3C). As a result, the subsequent tests utilized the SBF@GO/SF/HA and 1.5SBF@GO/SF/HA composite membranes, each submerged for one day.

The membranes' mechanical strength is essential for tissue regeneration since they must maintain a stable healing area and surrounding tissues (Huang et al., 2019; Cho et al., 2020). The average tensile strength of the electrospun silk fibroin composite membrane has been reported to be greater (6.14 ± 1.21 MPa) than that of an electrospun silk fibroin membrane (1.99 ± 0.15 MPa). Gelatin and PCL membranes have tensile strengths of 2.6 MPa, with PCL being weaker at 7 MPa (Wang et al., 2015). This biomimetic technique, HA/SF nanocomposite microsphere, was integrated into the SF membrane to fabricate the

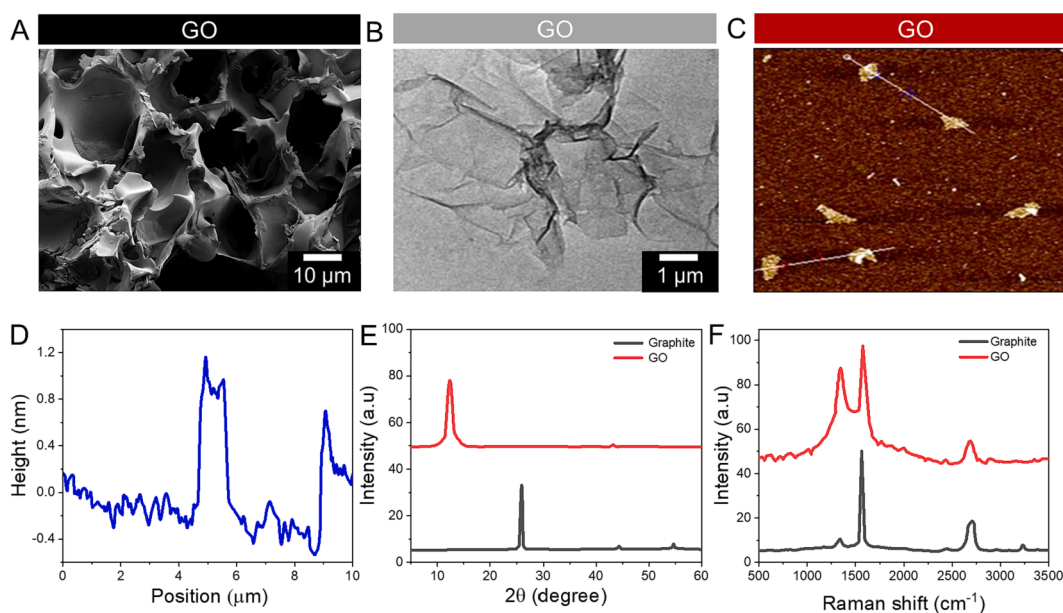


Fig. 1. GO nanosheet characterizations. A) SEM images of GO. B) TEM images of GO. C) AFM images of GO. D) AFM images of GO. E) XRD profile of GO and graphite. F) Raman spectral analysis of GO and graphite.

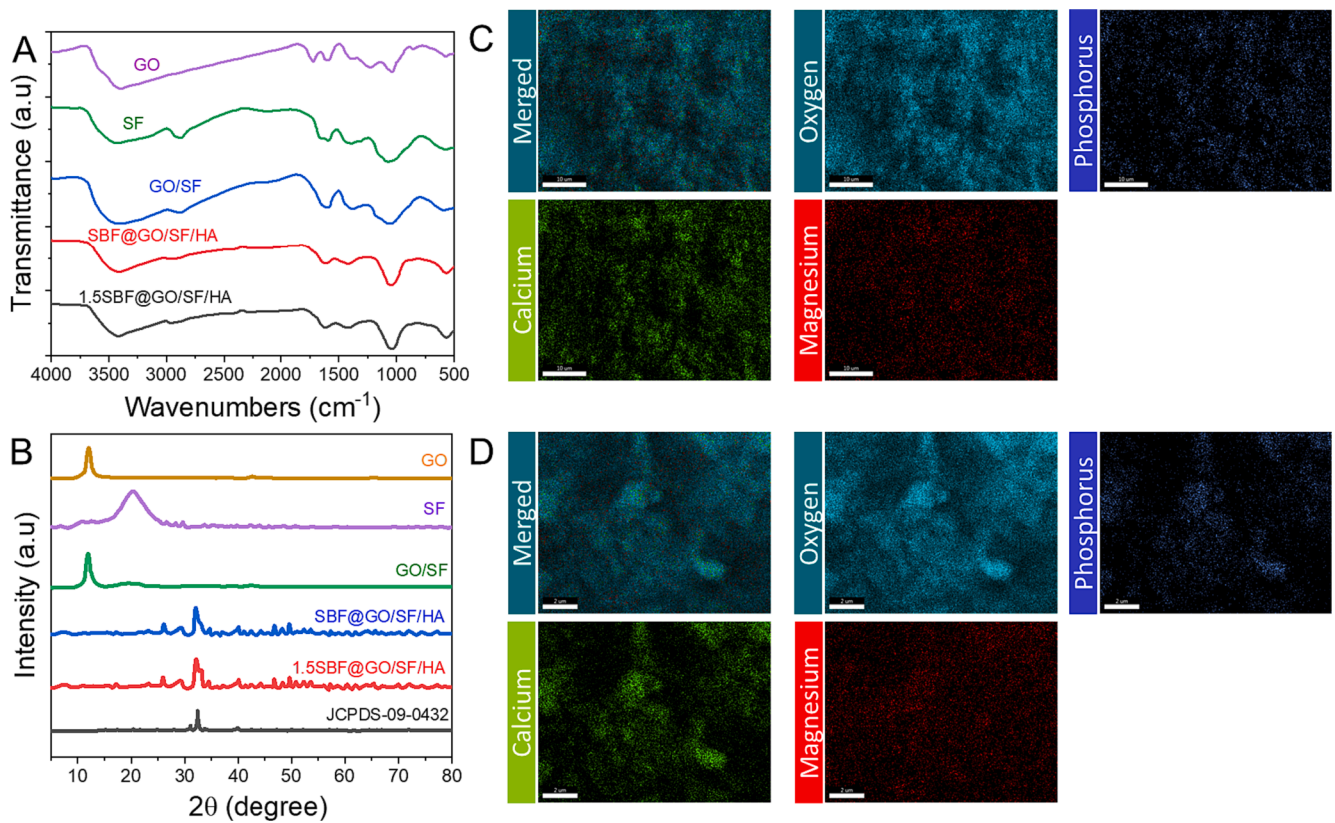


Fig. 2. Characterizations of GO, silk fibroin (SF), GO/SF, SBF@GO/SF/HA, 1.5SBF@GO/SF/HA, and JCPDS = 09-0432. A) FTIR spectral analysis. B) XRD spectral analysis. C) Elemental mapping analysis of SBF@GO/SF/HA. D) Elemental mapping analysis of 1.5SBF@GO/SF/HA.

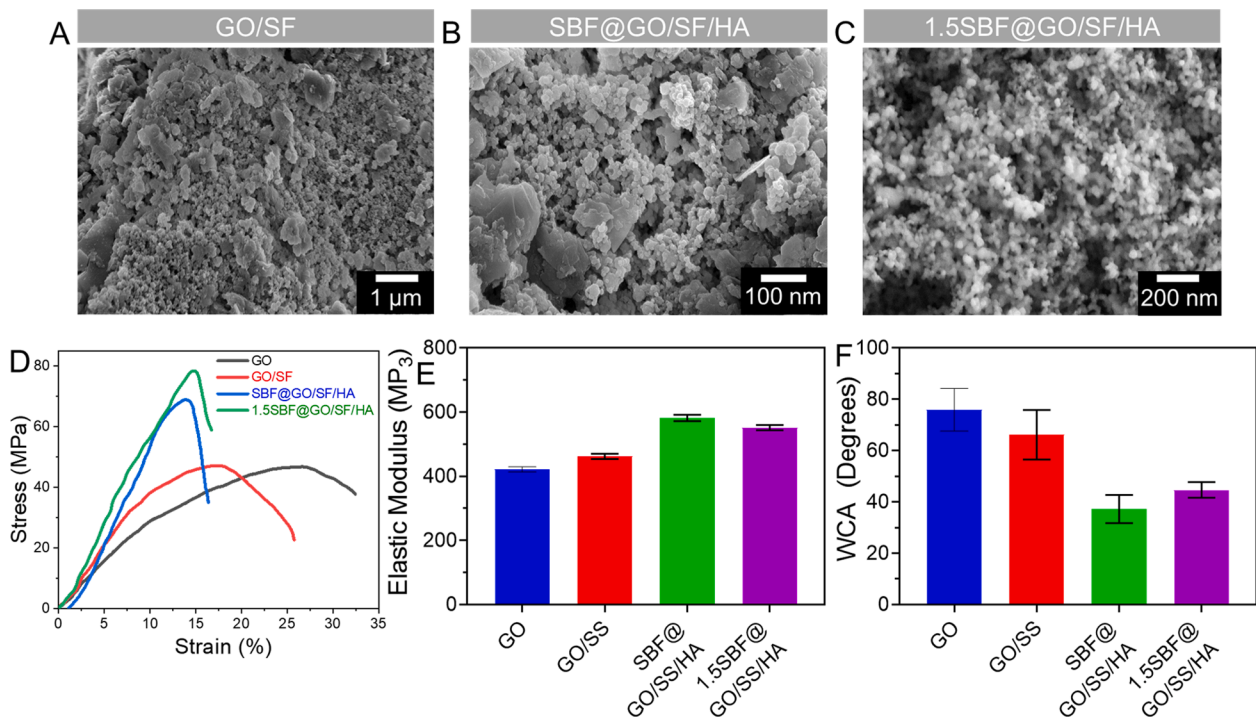


Fig. 3. Characterization of GO/SF, SBF@GO/SF/HA, and 1.5SBF@GO/SF/HA. A-C) SEM images of GO/SF, SBF@GO/SF/HA, and 1.5SBF@GO/SF/HA. Scale bar 1 μm and 200 nm. D) Stress-strain of GO, GO/SF, SBF@GO/SF/HA, and 1.5SBF@GO/SF/HA. E) Elastic modulus of GO, GO/SF, SBF@GO/SF/HA, and 1.5SBF@GO/SF/HA. F) Contact angle analysis of GO, GO/SF, SBF@GO/SF/HA, and 1.5SBF@GO/SF/HA. Data are presented as mean \pm standard deviation (SD).

nanocomposite microsphere membrane. The findings show that membranes with HA/SF microspheres have more excellent mechanical characteristics than membranes with pure SF microspheres or composite HA/SF microspheres. Over this, the tensile strength of the GO-mediated membrane was examined (Fig. 3D). The stress–strain curve showed 45.01 ± 2.15 MPa and 45.52 ± 1.99 MPa tensile strengths for the GO/SF membranes. HA deposited on SBF@GO/SF/HA and 1.5SBF@GO/SF/HA membranes enhanced their tensile strengths to 68.12 ± 1.53 and 78.25 ± 3.01 MPa. Incorporating HA nanoparticles into GO/SF membranes improved their tensile strength. Comparing the tensile strength of the GO/SF/HA membranes to that of the other three, these findings show that they are the most vital membranes.

Consequently, they can handle more weight and maintain a solid repair area. As a material's elastic modulus rises, its rigidity increases, making it less prone to deformation (Xu et al., 2019). The GO membranes' elastic moduli were 433.52 ± 12.15 MPa, 458.25 ± 10.13 MPa, 570.25 ± 11.63 MPa, and 545.21 ± 12.72 MPa (Fig. 3E). There was a significant difference in elastic modulus across the three membranes. They could preserve their repair space by incorporating inorganic nanoparticles into the mechanical characteristics of GO/SF membranes. GO/SF membranes had a WCA of $64.73 \pm 4.5^\circ$, indicating they are more hydrophilic than the GO membranes. The WCAs of the GO/SF membranes were higher than those of the GO membranes (Fig. 3F). WCA values of SBF@GO/SF/HA and 1.5SBF@GO/SF/HA membranes for $33.9 \pm 2.9^\circ$ and $46.2 \pm 2.1^\circ$, respectively. This shows that mineral deposition can enhance membrane hydrophilicity. Adding HA increased the hydrophilic character of the membranes even further, allowing for cell attachment and proliferation.

3.3. Adhesion of cells on the membranes

Cell shape and the extracellular matrix play a role in developing osteoblasts into bone cells. Eukaryotic cells have an actin filament that has a diameter of 7 nm. It's a critical part of the cellular-ECM interaction because it keeps cells' morphology, mechanosensing, and mechano-transduction functions intact. Fibronectin, a key glycoprotein component of ECM, regulates cell adhesion, migration, matrix construction, and osteogenesis (Yin et al., 2018). Actin and fibronectin staining were used to study cell adherence and spread in this study. Compared to cells grown on other membranes, SBF@GO/SF/HA and 1.5SBF@GO/SF/HA membranes stretched and generated longer filopodia on the first day

(Fig. 4). On 3rd day, the number of cells had stuck to SBF@GO/SF/HA, and these adhesive cells had spread more on the membranes than in other groups. SBF@GO/SF/HA membranes showed more intense fibronectin immunofluorescence on the 3rd day of cell culture, as shown in Fig. 4, compared to different groups of cells. According to these findings, MG-63 cells attached and spread considerably over SBF@GO/SF/HA membranes, which may be attributable to the membranes' crinkled and thick surface, which is more favorable to cell adhesion and helpful in preserving cell shape.

3.4. Cell viability and osteogenic differentiation

To evaluate the effect of SBF@GO/SF/HA membrane on proliferation and osteogenic differentiation, MG-63 was cultured on the surfaces of the different samples (Manissorn et al., 2020). Then, the proliferation and viability of the MG-63 were assessed via live/dead cell staining and MTT assay (Fig. 5A). After 3 or 7 days of culture, we found that MG-63 seeded on GO, GO/SS, SBF@GO/SF/HA, and 1.5SBF@GO/SF/HA exhibited an improved cell density and spreading area, as well as more than renowned filopodia wings compared to those seeded on the samples (Fig. 5B). The MTT technique measured cell survival on the membranes after 1, 3, and 7 days of exposure. There was no difference in cell viability between the membranes and the control after one or three days. Cells on the membrane demonstrated a higher activity level than the control on the 7th day. According to Fig. 6A, all the tested membranes boosted MG-63 cells' ALP activity in the SBF@GO/SF/HA membrane compared to the rest of the groups. Detecting osteogenic differentiation in its latter stages is commonly accomplished by staining mineralized nodules with alizarin red. As illustrated in Fig. 6B, mineralized nodules were found in all four membrane groups at 21 days, with the SBF@GO/SF/HA membrane having the most significant mineralized rate in all the groups.

According to the histomorphological H&E of bone sections, the control group's bone tissue production was less complete than that of the Sham group, observed by the GO/SF group. In contrast, the bone formation of the GO/SF/HA group was completed more than that of the other two groups (Fig. 7). The GO/SF/HA group demonstrated less positive staining than the Sham group because of its matured bone tissue, comparable to the Sham group (Fig. 7). According to all these studies, SBF@GO/SF/HA membranes offer the best potential for healing bone defects. To fabricate SBF@GO/SF/HA membranes, they use

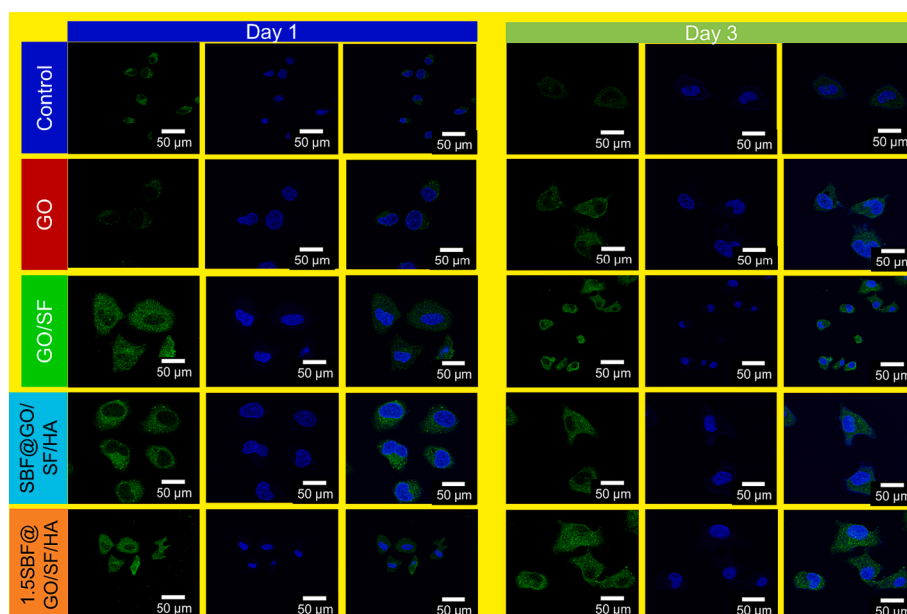


Fig. 4. Fibronectin image of MG-63 cells with GO, GO/SF, SBF@GO/SF/HA, and 1.5SBF@GO/SF/HA for days 1 and 3.

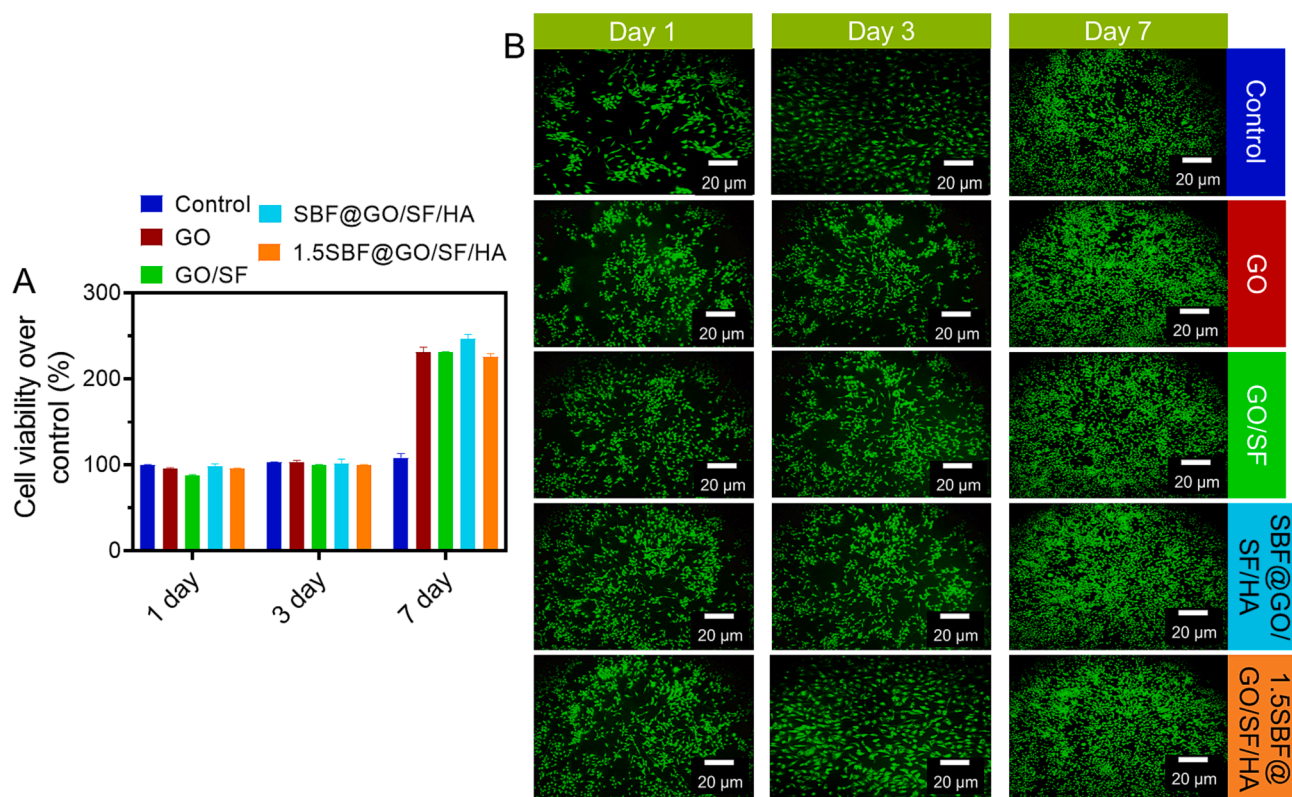


Fig. 5. Cell viability investigation. A) MG-63 cell viability of GO, GO/SF, SBF@GO/SF/HA, and 1.5SBF@GO/SF/HA for days 1, 3, and 7. Data are presented as mean \pm standard deviation (SD). B) Fluorescence imaging of respective samples. Scale bar 20 μ m.

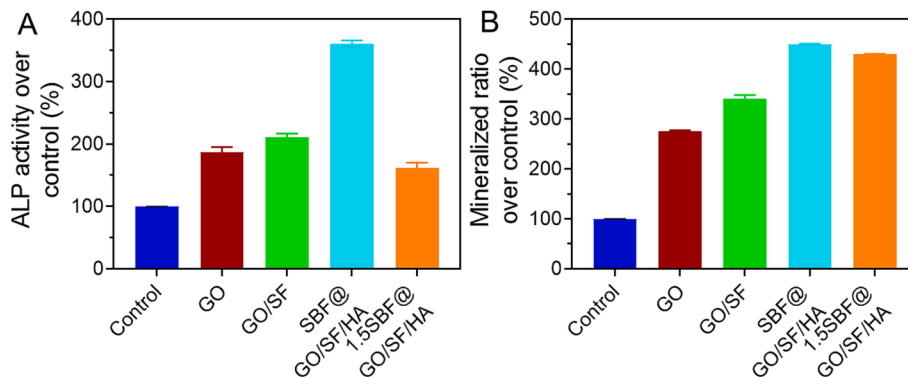


Fig. 6. Results of various membranes on differentiation of MG-63 cells. A) ALP activity of the cells on day 7. B) The mineralized matrix nodules of MG-63 cells on day 21. Data are presented as mean \pm standard deviation (SD).

biomimetic mineralization HA for bone regeneration.

3.5. Biosafety evaluation

In bone regeneration, 2D membrane biosafety is also crucial. A critical criterion in materials safety studies is blood compatibility, which measures how blood reacts to foreign chemicals. These membranes' hemolysis rates were below the national norm (5 %), indicating well-suited use with human blood (Fig. 8). Rats with SD were used for the histology experiments using SD subcutaneous tissue. One month after subcutaneous implantation, it took all groups to recover fully from the surgical scarring on their backs. Further, we examined the major organs (heart, liver, kidney, spleen, and lung), showing no significant changes compared to the sham group. The histomorphological image of the tissues and cell organization in the GO/SF and GO/SF/HA groups were identical (Fig. 9). These studies have satisfactorily demonstrated the

biocompatibility and safety of these composite membranes for application in biomedicine.

4. Conclusions

The biomimetic mineralization process and one-step vacuum filtering successfully fabricated GO/SF/HA composite membranes. For example, SBF@GO/SF/HA membranes have excellent mechanical characteristics, with tensile strength, elastic modulus, and hydrophilicity superior to conventional membranes. Osteogenic MG-63 cells adhered better to the SBF@GO/SF/HA membranes because of the roughened surface of the GO/SF/HA membranes. Another study found that SBF@GO/SF/HA showed the most vital osteogenic differentiation of MG-63 cells, with enhanced ALP activity, and mineralization. Several studies have shown this type of membrane expedites bone growth in vivo and has no detrimental effect on normal epidermal tissue. In this

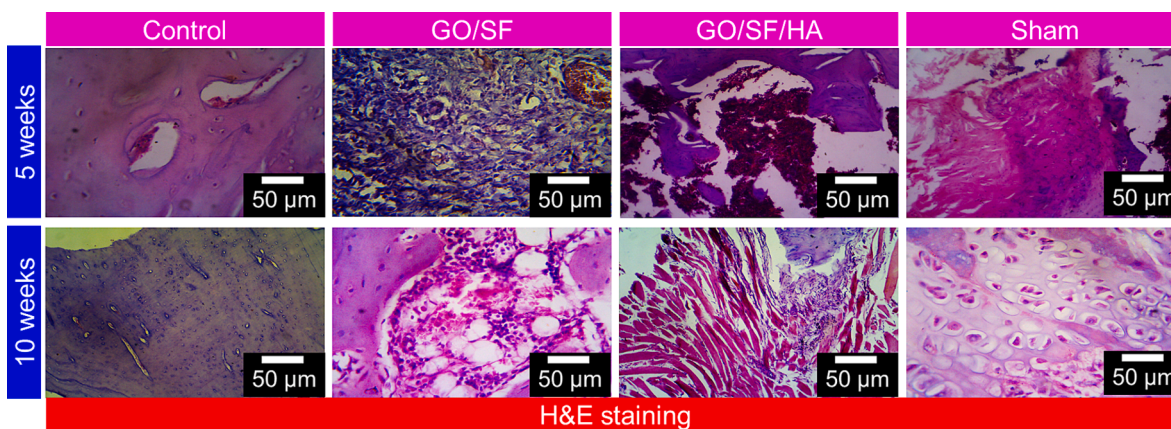


Fig. 7. Histological images of GO/SF, GO/SF/HA, and sham of bone generation after implantation for 5 and 10 weeks. Scale bar 50 μm .

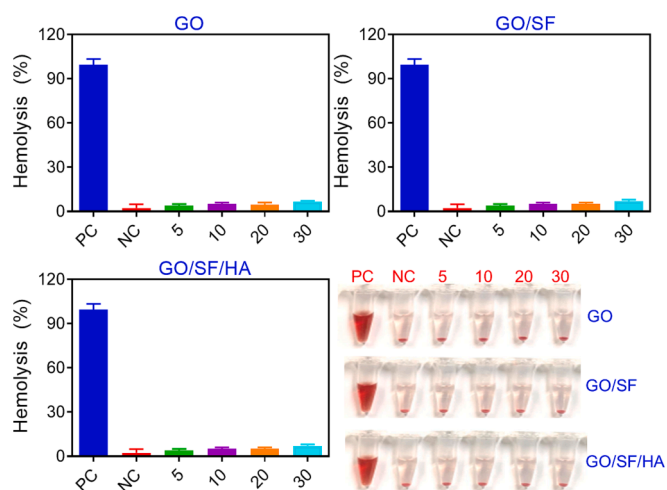


Fig. 8. Hemolysis ratio assessment of GO, GO/SF, GO/SF/HA membranes. Data are presented as mean \pm standard deviation (SD).

regard, SBF@GO/SF/HA membranes can be used to construct two-dimensional membrane materials for bone regeneration.

5. Financial & competing interests disclosure

This work was supported by Yunnan Orthopedics and Sports

Rehabilitation Clinical Medicine Research Center (Grant No.202102AA310068). The authors also extend their appreciation to the Researchers Supporting Project number (RSPD2023R677), King Saud University, Riyadh, Saudi Arabia, for financial support.

6. Ethical approval statement

All animal experiments were conducted under the supervision of the Animal Ethics Committee of the Department of Orthopedics, The First Affiliated Hospital of Kunming Medical University, Kunming, 650000, China, and strictly followed the NIH guidelines for the care and use of experiment animals. All experimental animals were housed in poly-acrylic cages under standard laboratory conditions, temperature of 20–22 $^{\circ}\text{C}$, and humidity of 65 % and maintained under a 12/12 h light/dark cycle. Animals received water and food ad libitum and were anesthetized with 2 % isoflurane inhalation. All authors have read the manuscript and consent for publication.

CRediT authorship contribution statement

Xi Li: Conceptualization, Writing – original draft, Project administration, Writing – review & editing. **Abdurahman Hajinur Hirad:** Data curation, Software, Writing – original draft, Methodology. **Rameshku-mar Santhanam:** Software, Data curation, Methodology, Writing – review & editing.

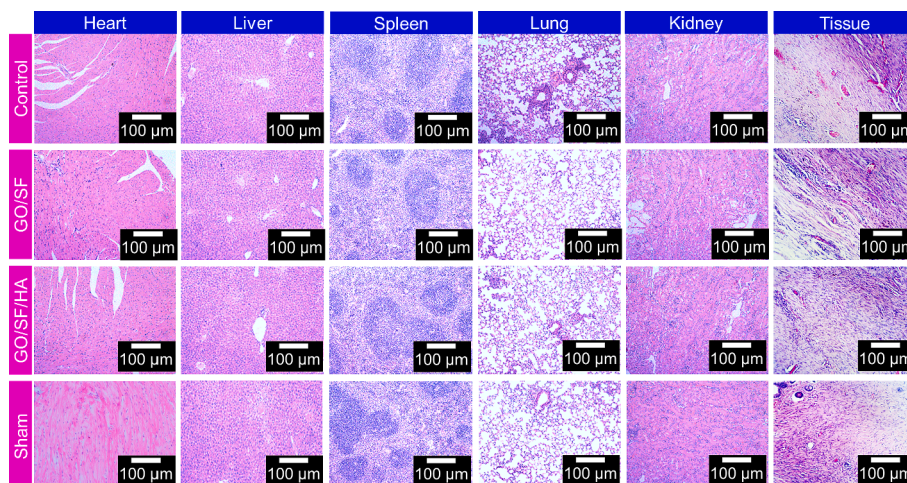


Fig. 9. H&E images of the main organs and subcutaneous tissue treated with GO/SF, GO/SF/HA, and sham. Scale bar 100 μm .

Declaration of competing interest

The authors declare that they have no known competing financial interests or personal relationships that could have appeared to influence the work reported in this paper.

References

- Abbasi, N., Hamlet, S., Love, R.M., Nguyen, N.-T., 2020. Porous scaffolds for bone regeneration. *J. Sci.: Adv. Mater. Devices* 5, 1–9.
- Alemi, F., Zarezadeh, R., Sadigh, A.R., Hamishehkar, H., Rahimi, M., Majidinia, M., Asemi, Z., Ebrahimi-Kalan, A., Yousefi, B., Rashtchizadeh, N., 2020. Graphene oxide and reduced graphene oxide: Efficient cargo platforms for cancer theranostics. *J. Drug Delivery Sci. Technol.* 60, 101974 <https://doi.org/10.1016/j.jddst.2020.101974>.
- Amiryaghoobi, N., Fathi, M., Barzegari, A., Barar, J., Omidian, H., Omid, Y., 2021. Recent advances in polymeric scaffolds containing carbon nanotube and graphene oxide for cartilage and bone regeneration. *Mater. Today Commun.* 26, 102097.
- Armiento, A.R., Hatt, L.P., Sanchez Rosenberg, G., Thompson, K., Stoddart, M.J., 2020. Functional biomaterials for bone regeneration: a lesson in complex biology. *Adv. Funct. Mater.* 30, 1909874.
- Azerbaijan, M.H., Bahmani, E., Jouybari, M.H., Hassaniazardaryani, A., Goleij, P., Akrami, M., Irani, M., 2021. Electrospun gold nanorods/graphene oxide loaded-core-shell nanofibers for local delivery of paclitaxel against lung cancer during photodynamic therapy method. *Eur. J. Pharm. Sci.* 164, 105914 <https://doi.org/10.1016/j.ejps.2021.105914>.
- Bagchi, A., Meka, S.R.K., Rao, B.N., Chatterjee, K., 2014. Perovskite ceramic nanoparticles in polymer composites for augmenting bone tissue regeneration. *Nanotechnology* 25, 485101.
- Bai, X., Gao, M., Syed, S., Zhuang, J., Xu, X., Zhang, X.-Q., 2018. Bioactive hydrogels for bone regeneration. *Bioact. Mater.* 3, 401–417.
- Bai, S., Zhang, X., Lv, X., Zhang, M., Huang, X., Shi, Y., Lu, C., Song, J., Yang, H., 2020. Bioinspired mineral-organic bone adhesives for stable fracture fixation and accelerated bone regeneration. *Adv. Funct. Mater.* 30, 1908381.
- Cheng, Y., Koh, L.-D., Li, D., Ji, B., Zhang, Y., Yeo, J., Guan, G., Han, M.-Y., Zhang, Y.-W., 2015. Peptide-graphene interactions enhance the mechanical properties of silk fibroin. *ACS Appl. Mater. Interfaces* 7, 21787–21796. <https://doi.org/10.1021/acsami.5b05615>.
- Cho, B.-G., Joshi, S.R., Lee, J., Park, Y.-B., Kim, G.-H., 2020. Direct growth of thermally reduced graphene oxide on carbon fiber for enhanced mechanical strength. *Compos. B Eng.* 193, 108010.
- Choe, G., Oh, S., Seok, J.M., Park, S.A., Lee, J.Y., 2019. Graphene oxide/alginate composites as novel bioinks for three-dimensional mesenchymal stem cell printing and bone regeneration applications. *Nanoscale* 11, 23275–23285.
- Eivazzadeh-Keihan, R., Radinekiyan, F., Madanchi, H., Aliabadi, H.A.M., Maleki, A., 2020. Graphene oxide/alginate/silk fibroin composite as a novel biostructure with improved blood compatibility, less toxicity and enhanced mechanical properties. *Carbohydr. Polym.* 248, 116802.
- Feicht, P., Biskupek, J., Gorelik, T.E., Renner, J., Halbig, C.E., Maranska, M., Puchtler, F., Kaiser, U., Eigler, S., 2019. Brodie's or Hummers' method: oxidation conditions determine the structure of graphene oxide. *Chem.–Eur. J.* 25, 8955–8959.
- Feng, P., Jia, J., Peng, S., Yang, W., Bin, S., Shuai, C., 2020. Graphene oxide-driven interfacial coupling in laser 3D printed PEEK/PVA scaffolds for bone regeneration. *Virt. Phys. Prototyping* 15, 211–226.
- Fischer, D., Li, Y., Ahlemeyer, B., Krieglstein, J., Kissel, T., 2003. In vitro cytotoxicity testing of polycations: influence of polymer structure on cell viability and hemolysis. *Biomaterials* 24, 1121–1131. [https://doi.org/10.1016/S0142-9612\(02\)00445-3](https://doi.org/10.1016/S0142-9612(02)00445-3).
- Girraj, K., Mohamed Kasim, M.S., Balasubramaniam, K., Thangavel, S.K., Venkatesan, J., Suresh, S., Shanmugam, P., Karri, C., 2022. Various coordination modes of new coumarin Schiff bases toward Cobalt (III) ion: Synthesis, spectral characterization, in vitro cytotoxic activity, and investigation of apoptosis. *Appl. Organomet. Chem.* 36, e6536. <https://doi.org/10.1002/aoc.6536>.
- Gisbert-Garzarán, M., Gómez-Cerezo, M.N., Vallet-Regí, M., 2023. Targeting agents in biomaterial-mediated bone regeneration. *Int. J. Mol. Sci.* 24, 2007.
- Glenske, K., Donkiewicz, P., Köwitsch, A., Milosevic-Oljaca, N., Rider, P., Rofall, S., Franke, J., Jung, O., Smeets, R., Schnettler, R., 2018. Applications of metals for bone regeneration. *Int. J. Mol. Sci.* 19, 826.
- Huang, K., Gu, Z., Wu, J., 2020. Tofu-incorporated hydrogels for potential bone regeneration. *ACS Biomater. Sci. Eng.* 6, 3037–3045. <https://doi.org/10.1021/acsbomaterials.9b01997>.
- Huang, G., Huo, S., Xu, X., Chen, W., Jin, Y., Li, R., Song, P., Wang, H., 2019. Realizing simultaneous improvements in mechanical strength, flame retardancy and smoke suppression of ABS nanocomposites from multifunctional graphene. *Compos. B Eng.* 177, 107377.
- Jiao, D., Zheng, A., Liu, Y., Zhang, X., Wang, X., Wu, J., She, W., Lv, K., Cao, L., Jiang, X., 2021. Bidirectional differentiation of BMSCs induced by a biomimetic procallus based on a gelatin-reduced graphene oxide reinforced hydrogel for rapid bone regeneration. *Bioact. Mater.* 6, 2011–2028.
- Kalaiaaras, G., Mohamed Subarkhan, M., Fathima Safwana, C.K., Sruthi, S., Sathiya Kamatchi, T., Keerthana, B., Ashok Kumar, S.L., 2022. New organoruthenium(II) complexes containing N, X-donor (X = O, S) heterocyclic chelators: Synthesis, spectral characterization, in vitro cytotoxicity and apoptosis investigation. *Inorg. Chim. Acta* 535, 120863. <https://doi.org/10.1016/j.ica.2022.120863>.
- Lee, J., Byun, H., Madhurakatt Perikamana, S.K., Lee, S., Shin, H., 2019. Current advances in immunomodulatory biomaterials for bone regeneration. *Adv. Healthc. Mater.* 8, 1801106.
- Lee, C.-S., Singh, R.K., Hwang, H.S., Lee, N.-H., Kurian, A.G., Lee, J.-H., Kim, H.S., Lee, M., Kim, H.-W., 2023. Materials-based nanotherapeutics for injured and diseased bone. *Prog. Mater. Sci.* 101087.
- Manissorn, J., Wattanachai, P., Tonsomboon, K., Bumroongsakulawat, P., Damrongsakkul, S., Thongnuek, P., 2020. Osteogenic enhancement of silk fibroin-based bone scaffolds by forming hybrid composites with bioactive glass through GPTMS during sol-gel process. *Mater. Today Commun.*, 101730 <https://doi.org/10.1016/j.mtcomm.2020.101730>.
- Metwally, S., Ferraris, S., Spriano, S., Krysiak, Z.J., Kaniuk, L., Marzec, M.M., Kim, S.K., Szewczyk, P.K., Gruszczynski, A., Wyrwal-Sarna, M., 2020. Surface potential and roughness controlled cell adhesion and collagen formation in electrospun PCL fibers for bone regeneration. *Mater. Des.* 194, 108915.
- Moe, Y.M., Nuntanarant, T., Khangkhamano, M., Meesane, J., 2022. Layer-by-layer particle deposited membranes of silk fibroin and poly (vinyl alcohol) for guided bone regeneration: molecular structure, morphology, and properties. *Mater. Technol.* 37, 332–344.
- Mohamed Kasim, M.S., Sundar, S., Rengan, R., 2018. Synthesis and structure of new binuclear ruthenium(II) arene benzil bis(benzoylhydrazone) complexes: Investigation on antiproliferative activity and apoptosis induction. *Inorganic Chemistry. Frontiers*, 5, 585–596. <https://doi.org/10.1039/c7q00761b>.
- Narimani, M., Teimouri, A., Shahbazarab, Z., 2019. Synthesis, characterization and biocompatible properties of novel silk fibroin/graphene oxide nanocomposite scaffolds for bone tissue engineering application. *Polym. Bull.* 76, 725–745.
- O'Neill, E., Awale, G., Daneshmandi, L., Umerah, O., Lo, K.-W.-H., 2018. The roles of ions on bone regeneration. *Drug Discov. Today* 23, 879–890.
- Ou, L., Lan, Y., Peng, Z., Feng, L., Yang, J., Liu, Y., Bian, L., Tan, J., Lai, R., Guo, R., 2019. Functionalization of SF/HAP Scaffold with GO-PEI-miRNA inhibitor complexes to enhance bone regeneration through activating transcription factor 4. *Theranostics* 9, 4525.
- Sathiya Kamatchi, T., Mohamed Subarkhan, M.K., Ramesh, R., Wang, H., Malecki, J.G., 2020. Investigation into antiproliferative activity and apoptosis mechanism of new arene Ru(II) carbazole-based hydrazone complexes. *Dalton Trans.* 49, 11385–11395. <https://doi.org/10.1039/D0DT01476A>.
- Sbricoli, L., Guazzo, R., Annunziata, M., Gobatto, L., Bressan, E., Nastro, L., 2020. Selection of collagen membranes for bone regeneration: a literature review. *Materials* 13, 786.
- Shuai, C., Yang, W., He, C., Peng, S., Gao, C., Yang, Y., Qi, F., Feng, P., 2020. A magnetic micro-environment in scaffolds for stimulating bone regeneration. *Mater. Des.* 185, 108275.
- Subarkhan, M.K.M., Ramesh, R., 2016. Ruthenium(II) arene complexes containing benzhydrazone ligands: Synthesis, structure and antiproliferative activity. *Inorg. Chem. Front.* 3, 1245–1255. <https://doi.org/10.1039/c6q00197a>.
- Samathra, M., Sadasivuni, K.K., Kumar, S.S., Rajan, M., 2018. Cisplatin-loaded graphene oxide/chitosan/hydroxyapatite composite as a promising tool for osteosarcoma-affected bone regeneration. *ACS Omega* 3, 14620–14633.
- Sun, J., Shakya, S., Gong, M., Liu, G., Wu, S., Xiang, Z., 2019. Combined application of graphene-family materials and silk fibroin in biomedicine. *ChemistrySelect* 4, 5745–5754.
- Sun, J., Li, L., Xing, F., Yang, Y., Gong, M., Liu, G., Wu, S., Luo, R., Duan, X., Liu, M., 2021. Graphene oxide-modified silk fibroin/nanohydroxyapatite scaffold loaded with urine-derived stem cells for immunomodulation and bone regeneration. *Stem Cell Res. Ther.* 12, 1–20.
- Takeuchi, R., Katagiri, W., Endo, S., Kobayashi, T., 2019. Exosomes from conditioned media of bone marrow-derived mesenchymal stem cells promote bone regeneration by enhancing angiogenesis. *PLoS One* 14, e0225472.
- Vimalraj, S., 2020. Alkaline phosphatase: Structure, expression and its function in bone mineralization. *Gene* 754, 144855.
- Wang, L., Fang, M., Xia, Y., Hou, J., Nan, X., Zhao, B., Wang, X., 2020. Preparation and biological properties of silk fibroin/nano-hydroxyapatite/graphene oxide scaffolds with an oriented channel-like structure. *RSC Adv.* 10, 10118–10128.
- Wang, S., Jiang, D., Zhang, Z., Chen, Y., Yang, Z., Zhang, J., Shi, J., Wang, X., Yu, J., 2019. Biomimetic nanosilica-collagen scaffolds for in situ bone regeneration: toward a cell-free, one-step surgery. *Adv. Mater.* 31, 1904341.
- Wang, W., Liu, Y., Yang, C., Jia, W., Qi, X., Liu, C., Li, X., 2020. Delivery of salvianolic acid B for efficient osteogenesis and angiogenesis from silk fibroin combined with graphene oxide. *ACS Biomater. Sci. Eng.* 6, 3539–3549.
- Wang, L., Lu, R., Hou, J., Nan, X., Xia, Y., Guo, Y., Meng, K., Xu, C., Wang, X., Zhao, B., 2020. Application of injectable silk fibroin/graphene oxide hydrogel combined with bone marrow mesenchymal stem cells in bone tissue engineering. *Colloids Surf. A Physicochem. Eng. Asp.* 604, 125318.
- Wang, S., Wang, C., Chen, H., 2020. MicroRNAs are critical in regulating smooth muscle cell mineralization and apoptosis during vascular calcification. *J. Cell Mol. Med.* 24, 13564–13572.
- Wang, B., Yuan, S., Xin, W., Chen, Y., Fu, Q., Li, L., Jiao, Y., 2021. Synergic adhesive chemistry-based fabrication of BMP-2 immobilized silk fibroin hydrogel functionalized with hybrid nanomaterial to augment osteogenic differentiation of rBMSCs for bone defect repair. *Int. J. Biol. Macromol.* 192, 407–416.
- Wang, S., Zhong, S., Lim, C.T., Nie, H., 2015. Effects of fiber alignment on stem cells-fibrous scaffold interactions. *J. Mater. Chem. B* 3, 3358–3366. <https://doi.org/10.1039/C5TB00026B>.
- Wessing, B., Lettner, S., Zechner, W., 2018. Guided bone regeneration with collagen membranes and particulate graft materials: a systematic review and meta-analysis. *Int. J. Oral Maxillofac. Implants* 33, 87–100.

- Wongpinyochit, T., Vassileiou, A.D., Gupta, S., Mushrif, S.H., Johnston, B.F., Seib, F.P., 2019. Unraveling the impact of high-order silk structures on molecular drug binding and release behaviors. *J. Phys. Chem. Lett.* 10, 4278–4284. <https://doi.org/10.1021/acs.jpcclett.9b01591>.
- Wright, Z.M., Arnold, A.M., Holt, B.D., Eckhart, K.E., Sydlik, S.A., 2019. Functional graphenic materials, graphene oxide, and graphene as scaffolds for bone regeneration. *Regener. Eng. Transl. Med.* 5, 190–209.
- Wu, T., Li, B., Huang, W., Zeng, X., Shi, Y., Lin, Z., Lin, C., Xu, W., Xia, H., Zhang, T., 2022. Developing a novel calcium magnesium silicate/graphene oxide incorporated silk fibroin porous scaffold with enhanced osteogenesis, angiogenesis and inhibited osteoclastogenesis. *Biomed. Mater.* 17, 35012.
- Wu, J., Zheng, A., Liu, Y., Jiao, D., Zeng, D., Wang, X., Cao, L., Jiang, X., 2019. Enhanced bone regeneration of the silk fibroin electrospun scaffolds through the modification of the graphene oxide functionalized by BMP-2 peptide. *Int. J. Nanomed.* 14, 733.
- Xu, C., Dai, G., Hong, Y., 2019. Recent advances in high-strength and elastic hydrogels for 3D printing in biomedical applications. *Acta Biomater.* 95, 50–59. <https://doi.org/10.1016/j.actbio.2019.05.032>.
- Yin, H., Wang, Y., Sun, X., Cui, G., Sun, Z., Chen, P., Xu, Y., Yuan, X., Meng, H., Xu, W., Wang, A., Guo, Q., Lu, S., Peng, J., 2018. Functional tissue-engineered microtissue derived from cartilage extracellular matrix for articular cartilage regeneration. *Acta Biomater.* 77, 127–141. <https://doi.org/10.1016/j.actbio.2018.07.031>.
- Zhai, P., Peng, X., Li, B., Liu, Y., Sun, H., Li, X., 2020. The application of hyaluronic acid in bone regeneration. *Int. J. Biol. Macromol.* 151, 1224–1239.
- Zhang, C., Shao, H., Luo, J., Hu, X., Zhang, Y., 2018. Structure and interaction of silk fibroin and graphene oxide in concentrated solution under shear. *Int. J. Biol. Macromol.* 107, 2590–2597. <https://doi.org/10.1016/j.ijbiomac.2017.10.142>.
- Zhang, D., Wu, X., Chen, J., Lin, K., 2018. The development of collagen based composite scaffolds for bone regeneration. *Bioact. Mater.* 3, 129–138.
- Zhao, S., Ma, P., Wan, A., Huang, J., Yu, H., Lai, E., Lin, H., Miao, X., Yue, X., 2021. The fabrication of cassava silk fibroin-based composite film with graphene oxide and chitosan quaternary ammonium salt as a biodegradable membrane material. *Autex Res. J.* 21, 459–466.
- Zheng, Z., Chen, Y., Hong, H., Shen, Y., Wang, Y., Sun, J., Wang, X., 2021. The “Yin and Yang” of immunomodulatory magnesium-enriched graphene oxide nanoscrolls decorated biomimetic scaffolds in promoting bone regeneration. *Adv. Healthc. Mater.* 10, 2000631.
- Zhu, T., Cui, Y., Zhang, M., Zhao, D., Liu, G., Ding, J., 2020. Engineered three-dimensional scaffolds for enhanced bone regeneration in osteonecrosis. *Bioact. Mater.* 5, 584–601.
- Zhu, L., Luo, D., Liu, Y., 2020. Effect of the nano/microscale structure of biomaterial scaffolds on bone regeneration, *International. J. Oral Sci.* 12, 1–15.